Enhancement of Mechanical and Thermal Insulation Properties of Polyvinyl Chloride Foam Using Leather Shavings

by
Chao Lei,[1,2] Weixing Xu,[1,3]* Bi Shi[1,3] and Yunhang Zeng[1,3]*
[1]*National Engineering Laboratory for Clean Technology of Leather Manufacture*, *Sichuan University*, Chengdu 610065, China
[2]*College of Biomass Science and Engineering*, *Sichuan University*, Chengdu 610065, China
[3]*Key Laboratory of Leather Chemistry and Engineering (Sichuan University)*, *Ministry of Education*, Chengdu 610065, China

Abstract

The global production of leather shavings (LSs) amounts to millions of tons annually, posing significant challenges in terms of resource waste and environmental pollution if not effectively managed. This study explores the utilization of LSs by fabricating modified leather fibers (MLFs) as reinforcing fillers to enhance the mechanical and thermal insulation properties of polyvinyl chloride (PVC) foams. The process involved pulverizing LSs and modifying them with a polyethylene glycol–isophorone diisocyanate (PEG–IPDI) prepolymer to create MLF. This MLF was then incorporated into PVC to produce MLF/PVC foam. The PEG–IPDI prepolymer modification aligned the surface free energy of MLF (33.82 ± 1.97 mJ/m^2) with that of PVC (31.08 ± 3.65 mJ/m^2), thereby improving their interfacial compatibility and imparting thermal energy storage capacity to the MLF. The resulting MLF/PVC foam exhibited enhancements in compressive strength and modulus, showing increases of 93.7% and 165.8%, respectively, compared to pure PVC foam. Furthermore, MLF/PVC foam demonstrated a slower surface temperature increase when heated using a heating plate at 110°C compared to pure PVC foam. These findings indicate that MLF enhances the mechanical and thermal insulation properties of PVC foams, primarily due to the improved foaming and thermal storage capacities imparted by the MLF.

Introduction

The leather industry significantly contributes to the global economy, with its trade value estimated at approximately $400 billion annually.[1] However, it also generates millions of tons of leather shavings (LSs) worldwide each year. These LSs can lead to substantial resource waste and environmental pollution if not treated properly.[2-3] Currently, LSs are primarily utilized for extracting collagen and its hydrolysate, or for producing adsorbents,[4] conductive materials,[5] and reinforcing fillers.[6-9] These applications often involve simple processing methods. LSs are rich in leather fibers (LFs) that have a multidirectional and hierarchical structure from collagen fibrils to collagen fibers and further to collagen fiber bundles. This structure potentially enhances the mechanical properties of polymers.[6-9] Thus, employing LF as reinforcing fillers in polymer-based composites presents a viable approach for LS resource utilization.

Polyvinyl chloride (PVC), a widely used commercial polymer, is known for its excellent flame retardancy, chemical resistance, and affordability.[10] Specifically, foamed PVC, characterized by its lightweight nature, water resistance, and thermal insulation properties, finds applications in construction, transportation, and packaging.[11] However, linear PVC typically exhibits poor foaming capacity, primarily due to its low melt strength and viscoelasticity, which in turn affects the mechanical and thermal insulation properties of PVC foams.[12-14] Restricting the movement of PVC chains through cross-linking or filling is thought to be able to ameliorate the above defects. While filling PVC with materials such as calcium carbonate,[15] mica,[16] and graphene oxide[17] is an effective strategy to improve its foaming capacity, these fillers often fall short in improving mechanical and thermal insulation properties due to their simple structures and high thermal conductivity. In contrast, the complex structure and high porosity of LF can effectively restrict polymer chain movement while exhibiting low thermal conductivity.[6-7,18] Therefore, incorporating LF into PVC foams is expected to enhance the mechanical and thermal insulation properties of PVC foams.

As global energy efficiency standards intensify, there is a growing need for foams not only to provide thermal insulation but also to possess thermal energy storage capabilities to further conserve energy.[19] Phase change materials (PCMs) are pivotal in this context, as they can store or release substantial energy during their phase transition processes.[20] Integrating PCMs with foams has been shown to enhance the thermal insulation performance of the foams.[21] Among various PCMs, polyethylene glycol (PEG) is a notable solid–liquid PCM, recognized for its high latent heat, chemical stability, and thermal robustness. However, PEG is prone to leak during the phase change process and results in adverse effects on the surrounding environment.[22] A promising

*Corresponding author E-mail address: xuwx@scu.edu.cn (Weixing Xu), zengyunhang@scu.edu.cn (Yunhang Zeng).
Manuscript received January 29, 2024, accepted for publication February 27, 2024.

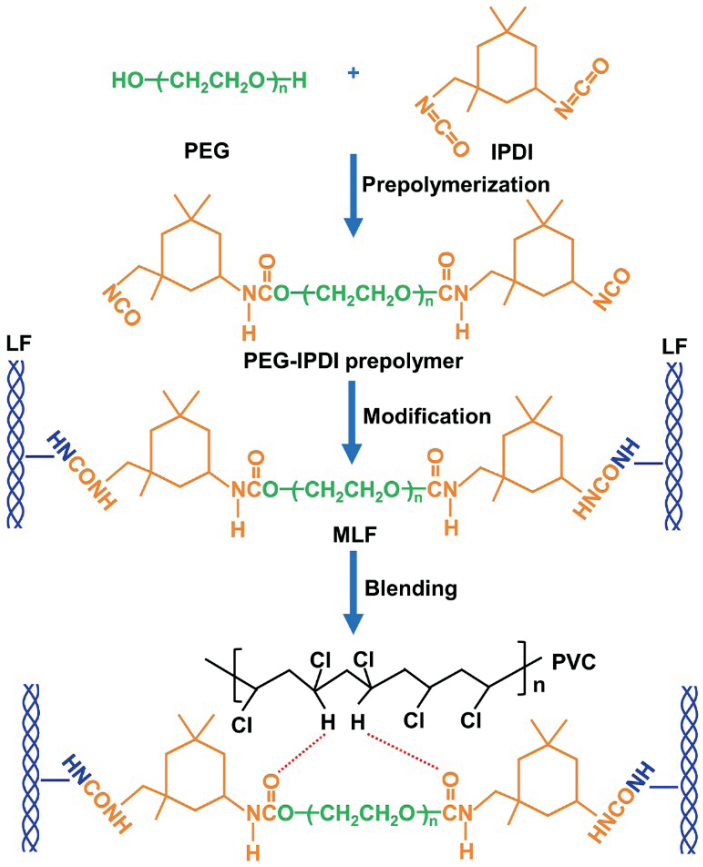

Figure 1. Schematic for the preparation of MLF and MLF/PVC foam.

solution to this issue is the conversion of PEG into a solid–solid PCM (SSPCM) using diisocyanate as a cross-linking agent and LF as a support material, which is expected to effectively mitigate leakage concerns.[23-24]

This study aims to facilitate the resource utilization of LS by employing LF as reinforcing fillers for fabricating PVC foams with superior mechanical and thermal insulation properties. LF, rich in hydrophilic groups such as –COOH, –NH_2, and –OH, exhibits poor interfacial compatibility with hydrophobic PVC.[8] Therefore, hydrophobic isophorone diisocyanate (IPDI)-capped PEG (PEG–IPDI) was used to chemically modify LF, improve the interfacial compatibility between LF and PVC, and endow LF with thermal energy storage capacity. The resulting modified LF (MLF) was then blended with PVC and foamed to produce MLF/PVC foam (Figure 1). A comparative analysis of the mechanical and thermal insulation properties of MLF/PVC foam was conducted against those of pure PVC foam, PEG–IPDI/PVC foam, and LF/PVC foam, focusing on rheological behavior, foaming capacity, and compressive and thermal properties.

Experimental

Materials

LSs were sourced from Senlu Leather Co., Ltd., Shandong, China. PEG with an average molecular weight (M_n) of 6000 g/mol, IPDI, N,N-dimethylformamide (DMF), dibutyltin dilaurate (DBTDL), and dioctyl phthalate (DOP) were acquired from Chengdu Chron Chemical Co., Ltd., Sichuan, China, and were of analytical grade. PVC (SG-5), obtained from Tianye Co., Ltd., Xinjiang, China, was of commercial quality. Barium stearate, cadmium stearate, Ca/Zn stabilizer, calcium stearate, polyethylene wax, and azodicarbonamide (AC) blowing agent, all commercial grade, were purchased from Winner New Material Technology Co., Ltd., Guangdong, China.

Preparation of MLF

Initially, the LS was thoroughly washed and neutralized to a pH of 7.0–8.0. After adequate dehydration and drying, it was pulverized using an ultra-centrifugal mill (ZM 200, Retsch, Germany) to produce LF with a size smaller than 40 mesh.

PEG was pre-dried under vacuum at 120°C for 2 h. In separate containers, 30 g (0.005 mol) of PEG and 2.225 g (0.01 mol) of IPDI were dissolved in DMF. The PEG solution was gradually added to the IPDI solution under stirring, followed by the addition of 1–2 drops of DBTDL as a catalyst. The reaction was conducted in a thermostatic oil bath at 60°C under a nitrogen atmosphere for 5 h, resulting in the formation of PEG–IPDI prepolymer with terminal isocyanate groups. Subsequently, 10 g of LF was incorporated into this prepolymer mixture and thoroughly blended. The combined mixture was then transferred to a vacuum oven and maintained at 60°C for 24 h to ensure complete cross-linking of the prepolymer with the LF. The resultant material was ground to achieve MLF of less than 40 mesh size. The grafting ratio of PEG–IPDI prepolymer to MLF was calculated using Equation (1):

$$\text{Grafting ratio} = (w_1 - w_0) \times 100/w_0, \quad (1)$$

where w_1 and w_0 represent the weights of LF before and after grafting with the PEG–IPDI prepolymer, respectively.

Preparation of PVC-based composite foams

The MLF, PVC, and various additives were homogeneously mixed using a high-speed mixer for 10 min, following the formulation presented in Table I. The blends were then melt-blended in a torque rheometer (RM-200C, Harp, China) at 135°C for 10 min. The MLF/PVC composite was subsequently hot-pressed at 150°C and 10 MPa for 10 min and foamed at 180°C for 5 min to produce the MLF/PVC foam. Control samples of PEG–IPDI/PVC foam and LF/PVC foam were prepared using an identical process, but MLF was substituted with PEG–IPDI prepolymer and LF, respectively.

Table I

Formulation of pure PVC and composite foams

Sample	Filler (per hundred/resin)	PVC (per hundred/resin)	Additives (per hundred/resin) [a]
PVC	0	100	21.3
PEG-IPDI/PVC	51.5 [b]	100	21.3
LF/PVC	25	100	21.3
MLF/PVC	25	100	21.3

[a] The additives comprised DOP (10 per hundred/resin), barium stearate (0.6 per hundred/resin), cadmium stearate (0.4 per hundred/resin), Ca/Zn stabilizer (6 per hundred/resin), calcium stearate (1 per hundred/resin), polyethylene wax (0.8 per hundred/resin), and AC blowing agent (2.5 per hundred/resin).

[b] The quantity of PEG–IPDI prepolymer in the PEG–IPDI/PVC foam corresponds to the amount grafted onto LF in the MLF/PVC foam.

Analyses of morphology and chemical structure

Morphological examination of the samples was observed using a scanning electron microscope (SEM; Apreo S HiVoc, FEI, USA). The chemical structures of the samples were analyzed using a Fourier transform infrared spectroscopy (FTIR; Nicolet iS 10, Thermo Fisher, USA). The binding energies of the elements on the sample surfaces were measured using an X-ray photoelectron spectroscopy (XPS; Thermo 250Xi, Thermo Scientific, USA). The contact angles of the samples were determined using a contact angle goniometer (DSA30, Krüss, Germany).

Analysis of rheological behavior

The rheological behavior of the samples was evaluated in an oscillatory mode using a rotational rheometer (MCR302, Anton Paar, Austria) equipped with a parallel-plate geometry (diameter = 25 mm, gap = 1 mm). Viscoelastic parameters were assessed through dynamic frequency scanning (0.01–100 rad/s) at 180 °C, maintaining a constant strain of 1% to ensure the linear viscoelastic range.

Analysis of foaming capacity

The mass densities of the samples were measured via the water displacement method, adhering to the ASTM D792-00 standard. The expansion ratio (*Φ)* was calculated using Equation (2):

$$\Phi = \rho_s/\rho_f, \quad (2)$$

where ρ_s and ρ_f represent the densities of the unfoamed and foamed samples, respectively. Pore diameter distributions were measured at 25°C using an automatic mercury intrusion porosimeter.

Testing of compressive properties

The compressive properties of the samples were tested using a universal testing machine (5967, INSTRON, USA), following the ASTM D695-02 standard.

Analysis of thermal energy storage capacity

The thermal energy storage capacities of the samples were evaluated using differential scanning calorimetry (DSC; DSC 204-F1, Netzsch, Germany). Each sample was subjected to a heating phase from 0°C to 80°C at a rate of 10°C/min, followed by cooling back to 0°C at the same rate.

The thermal reliability of the samples was assessed through an accelerated thermal cycling test. This involved repeatedly heating and cooling the samples between 20°C and 80°C for 100 and 200 cycles at a rate of 10°C/min. Post-cycling, the thermal properties of the samples were reanalyzed using DSC.

Testing of thermal insulation property

The thermal insulation performance of the samples was quantified by measuring their thermal conductivity. This measurement was performed using a transient plane source hot-disk thermal constants analyzer (TPS 2500 S, Hot Disk, Sweden). The samples were positioned on a heating plate set at 110°C, and infrared thermal imaging was conducted using an infrared imaging camera (T540, FLIR, USA).

Results and Discussion

Structure and properties of MLF

The primary objective of this research was to utilize the multidirectional and hierarchical structure of LF to enhance the mechanical and thermal insulation properties of PVC foams. The morphologies of LF and MLF were observed using SEM, as depicted in Figure 2a. The MLF retained a hierarchical structure similar to that of LF, ranging from collagen fibrils (50–200 nm) to collagen fibers (2–10 μm) and further to collagen fiber bundles (20–100 μm). This observation indicates that the unique structure of LF was preserved in MLF following modification with PEG–IPDI prepolymer.

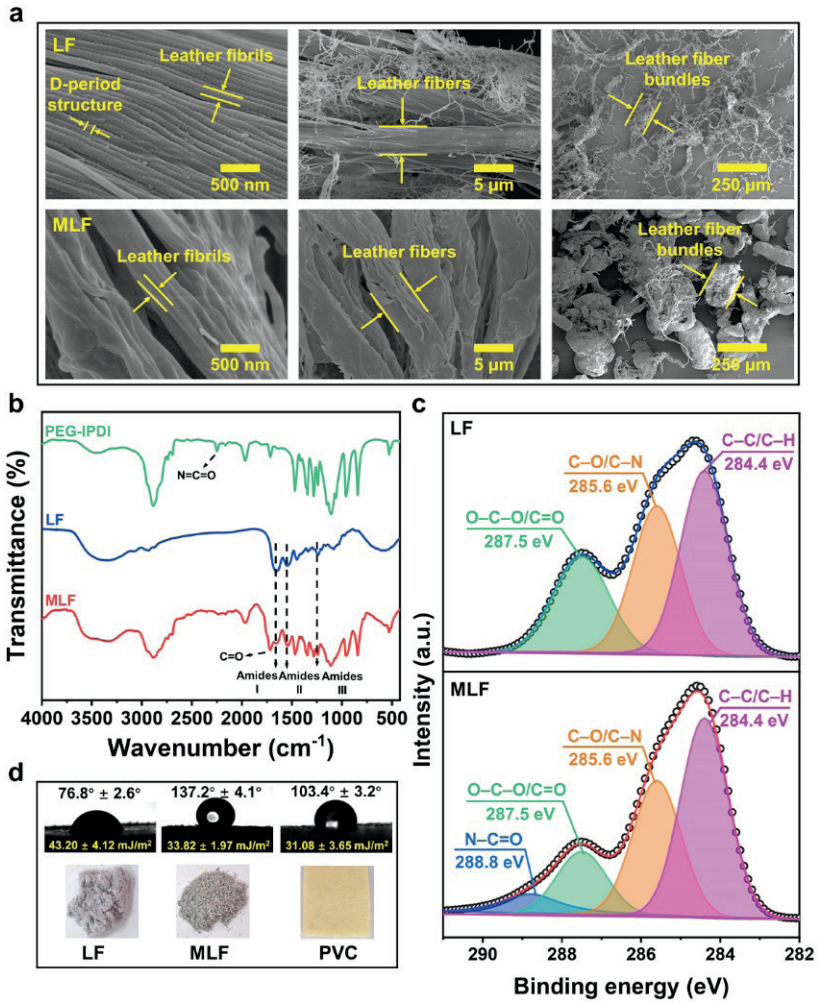

Figure 2. **(a)** SEM images; **(b)** FTIR spectra; **(c)** XPS C1s spectra; **(d)** water contact angles, surface free energies, and digital photos of LF and MLF.

The impact of PEG–IPDI prepolymer modification on MLF's chemical structure was analyzed using FTIR and XPS. Figure 2b shows the FTIR spectra of PEG–IPDI, LF, and MLF. The spectra of LF and MLF exhibited characteristic absorption peaks at 1655–1657, 1540–1544, and 1238–1242 cm^{-1}, corresponding to amides I, II, and III,[6,25-26] respectively, suggesting that the polypeptide chain structure of LF remained unaltered after modification. In the MLF spectrum, the disappearance of the N=C=O group's characteristic absorption peak at 2250 cm^{-1} (from PEG–IPDI) indicates a successful cross-linking reaction of the N=C=O groups of PEG–IPDI prepolymer with the $-NH_2$ groups of LF (Figure 1).[27] The peak at 1720 cm^{-1} in the MLF spectrum is attributed to the C=O stretching vibration of the PEG–IPDI prepolymer. The XPS analysis of the MLF surface, as shown in Figure 2c, reveals distinct features. The C1s spectrum of LF was decomposed and fitted into three peaks, centered at 284.4, 285.6, and 287.6 eV, corresponding to C–C/C–H, C–O/C–N, and O–C–O/C=O, respectively.[28] Following the modification of LF with PEG–IPDI prepolymer, the C1s spectrum of MLF shows four peaks: C–C/C–H (284.4 eV), C–O/C–N (285.6 eV), O–C–O/C=O (287.1 eV), and N–C=O (288.8 eV).[29] The appearance of N–C=O bonds in the MLF spectrum further confirms the successful grafting of PEG–IPDI prepolymer onto LF (Figure 1).

Water contact angles and surface free energies of LF, MLF, and PVC are presented in Figure 2d. The water contact angle of MLF increased to 137.2° ± 4.1°, compared to LF's 76.8° ± 2.6°, and approached that of PVC (103.4° ± 3.2°). Moreover, MLF's surface free energy (33.82 ± 1.97 mJ/m^2) was more aligned with PVC's (31.08 ± 3.65 mJ/m^2). These results suggest that the PEG–IPDI prepolymer effectively enhances the interfacial compatibility between LF and PVC, adhering to the principle of "like-dissolves-like."[30]

Interfacial structure of MLF/PVC

Effective interfacial compatibility between MLF and PVC is crucial for securing the mechanical and thermal insulation properties of MLF/PVC. The freeze-fractured surfaces of LF/PVC and MLF/PVC before foaming were observed using SEM to visually evaluate the interfacial compatibility between fillers and PVC. Figure 3a reveals noticeable gaps (highlighted with yellow circles) between LF and PVC, potentially hindering stress transfer between LF and PVC and preventing LF/PVC from fully utilizing LF's structural benefits. In contrast, minimal gaps were observed in the MLF/PVC composite, which can be attributed to the enhanced interfacial compatibility imparted by the PEG–IPDI prepolymer.

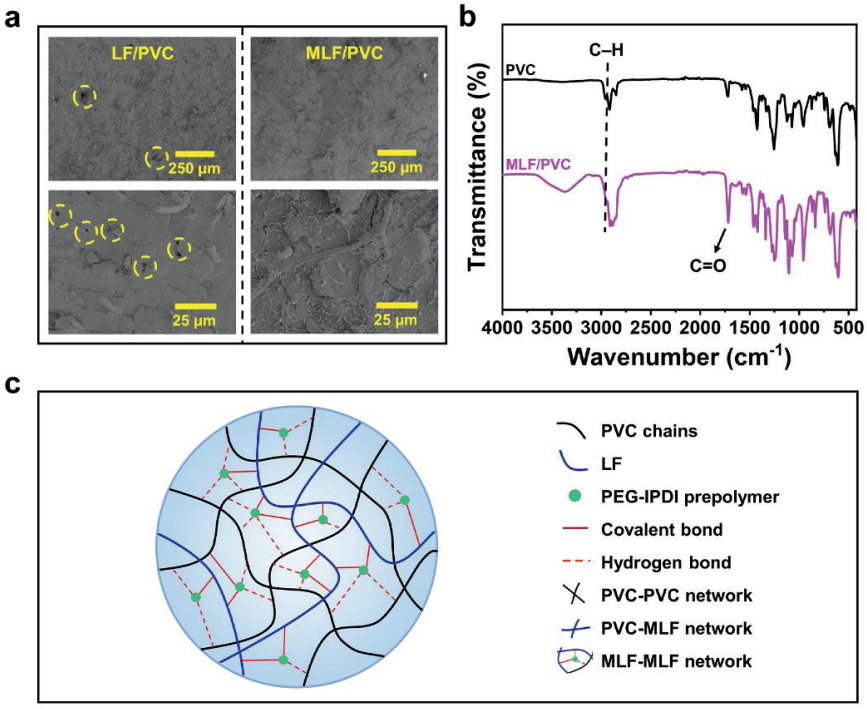

Figure 3. **(a)** SEM images of the surfaces of LF/PVC and MLF/PVC; **(b)** FTIR spectra of pure PVC and MLF/PVC; **(c)** schematic of the interaction between MLF and PVC.

The interfacial chemical structure of MLF/PVC was further analyzed by comparing the FTIR spectra of pure PVC and MLF/PVC. The FTIR spectrum of the MLF/PVC composite encompasses characteristic peaks of both MLF and pure PVC (Figures 2b and 3b). Notably, the C=O peak at 1716 cm^{-1} and the C–H peak at 2959 cm^{-1} in the MLF/PVC spectrum were shifted to lower wavenumbers compared to the C=O peak at 1720 cm^{-1} in MLF and the C–H peaks at 2952 cm^{-1} in pure PVC.[31-32] This shift suggests the possible formation of hydrogen bonds between the –NHCOO– groups of MLF and the C–H groups of PVC (Figure 1),[33] indicating that PEG–IPDI prepolymer enhances interfacial compatibility between MLF and PVC by forming interactions between MLF and PVC (Figure 3c). Improved interfacial compatibility between MLF and PVC is expected to more effectively utilize LF's structural advantages and enhance PVC's foaming capacity.

Rheological behavior of MLF/PVC

The rheological behavior of polymers is closely related to their melt strength and viscoelasticity, which is an important factor affecting their foaming capacity.[34] The variations in complex viscosity (η*), storage modulus (G′), loss modulus (G″), and loss tangent (tan δ) across dynamic frequencies for pure PVC and its composites are depicted in Figure 4. The η^* values of the four samples decreased with the increase in dynamic frequency, exhibiting the shear-thinning behavior of PVC melt (Figure 4a).[35] Pure PVC exhibited a lower η* value owing to weaker interactions among its chains, suggesting limited melt strength at the macroscopic level and, consequently, reduced foaming capacity. In contrast, PVC composites showed higher η^* values than pure PVC, attributable to the formation of various networks (PVC–PVC network, PVC–filler network, and filler–filler network) that impeded the movement of PVC chains (Figure 4a).[36] Notably, the η^* value of MLF/PVC was higher than that of LF/PVC (Figure 4a); this indicated that the more stable networks of MLF/PVC resisted the movement of the PVC chains more effectively compared to LF/PVC, thus greatly enhanced the strength of the PVC melt.[37]

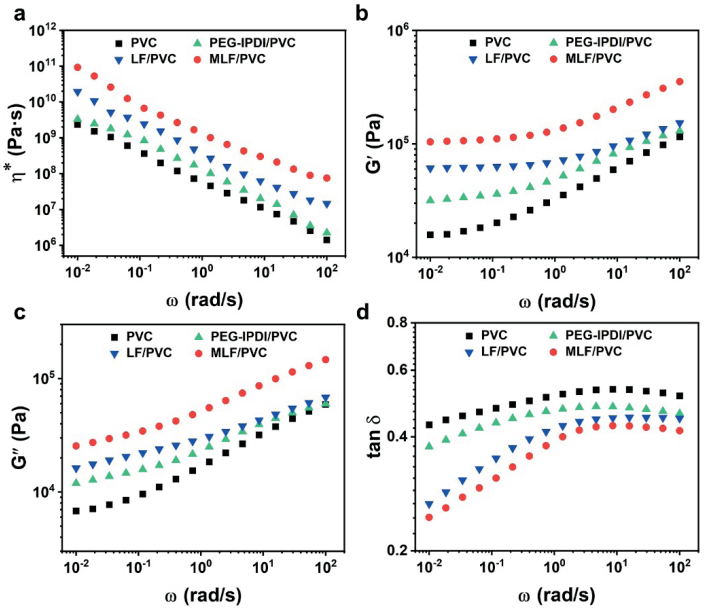

Figure 4. **(a)** Rheological behavior of pure PVC and composites: complex viscosity (η^*), **(b)** storage modulus (G′), **(c)** loss modulus (G″), and **(d)** loss tangent (tan δ).

G′ and G″ represent the energy stored and dissipated during deformation, respectively, and are crucial in determining the foaming behavior of PVC.[38] The G′ and G″ values of the samples were observed to follow the order MLF/PVC > LF/PVC > PEG–IPDI/PVC > pure PVC (Figure 4b and 4c). The order indicated that MLF/PVC had the highest elastic and viscous responses among the four samples. The loss tangent (tan δ = G″/G′) serves as an essential parameter for assessing polymer viscoelasticity.[38] The tan δ values of MLF/PVC exhibited the lowest value (Figure 4d), suggesting its superior viscoelasticity. In summary, MLF's multidirectional and hierarchical structure enhances the strength and viscoelasticity of PVC melt. This enhancement in melt strength and viscoelasticity is also expected to improve PVC's foaming capacity.

Foaming capacity of MLF/PVC

Foaming experiments were conducted on pure PVC, PEG–IPDI/PVC, LF/PVC, and MLF/PVC at 180°C for 5 min. To evaluate the influence of MLF on the foaming capacity of PVC, the microstructures and expansion ratios of the samples were analyzed. Figure 5a revealed that pure PVC foam exhibited large cell sizes and a low cell count, attributed to the low strength and viscoelasticity of the PVC melt. The inclusion of fillers (PEG-IPDI prepolymer, LF, and MLF) led to reduced cell sizes and increased cell counts in the PVC composite foams. Figures 5b–e show the pore diameter distributions of the samples. The MLF/PVC foam demonstrated superior properties, with the highest porosity (45.9%), smallest average pore diameter (30.2 μm), and lowest density (0.5323 g/cm^3). Furthermore, the expansion ratio of MLF/PVC foam increased by

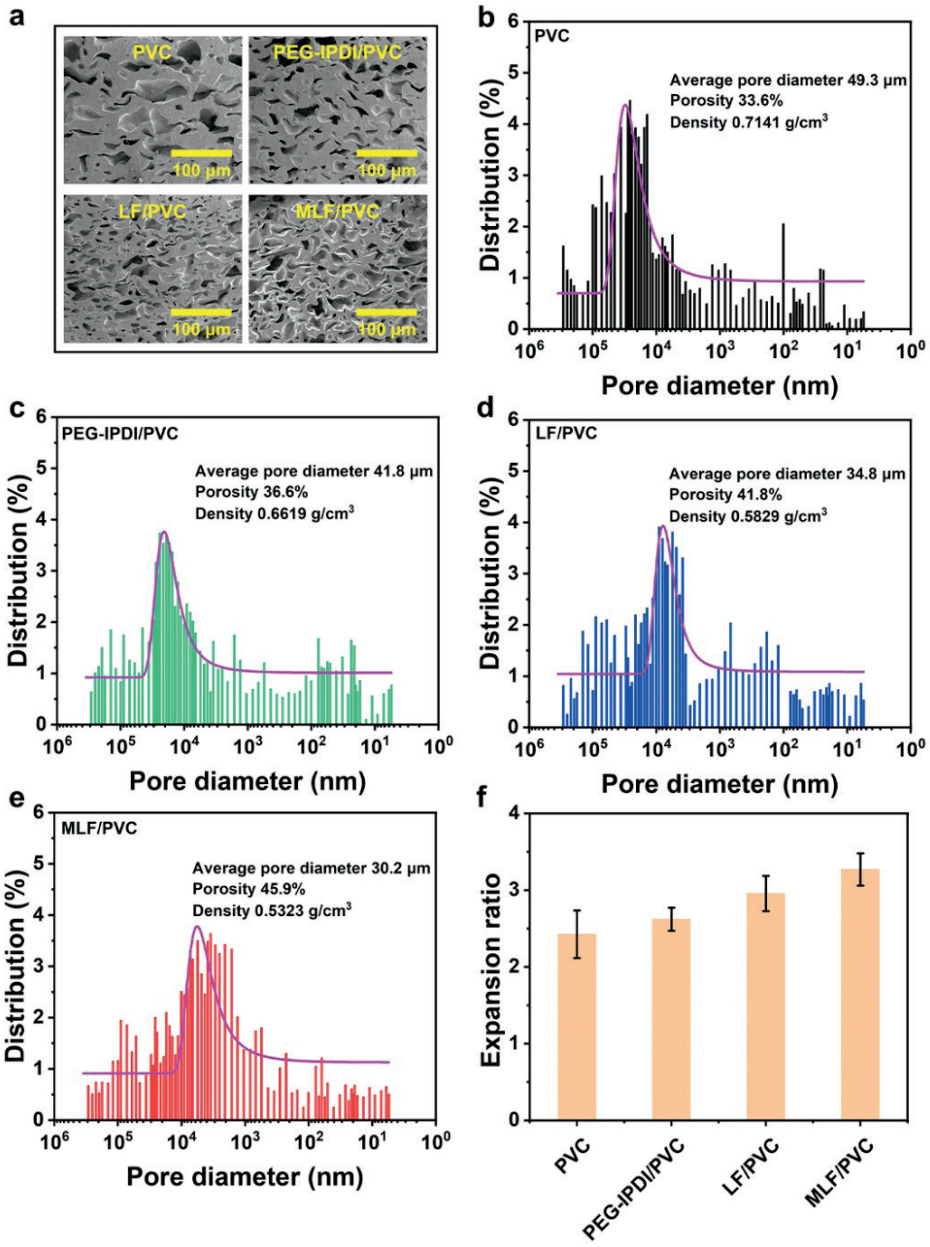

Figure 5. **(a)** Microstructures, **(b–e)** pore diameter distributions, and **(f)** expansion ratios of pure PVC and composite foams.

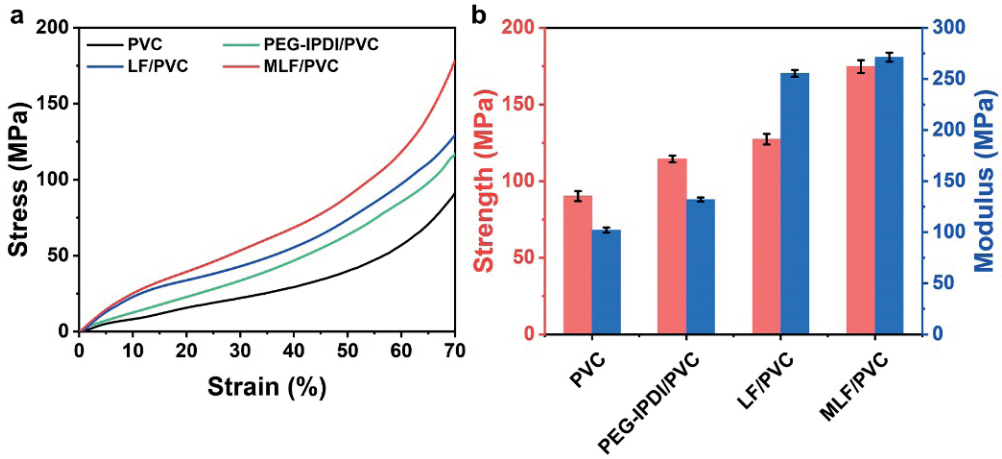

Figure 6. (a) Compressive stress–strain curves and **(b)** compressive strength and modulus of pure PVC and composite foams.

30.7% compared to that of pure PVC (Figure 5f). These findings indicate that MLF, with its multidirectional and hierarchical structure, greatly improves the foaming capacity of PVC owing to the improved strength and viscoelasticity of the PVC melt, which is expected to enhance the mechanical and thermal insulation properties of PVC foams.[12-14]

Mechanical properties of MLF/PVC foam

The compressive properties, crucial for assessing the mechanical performance of PVC foams, were evaluated.[39] Figure 6a presents the compressive stress–strain curves of pure PVC and the composite foams. All four samples exhibited no yield and maintained good ductility during compression. The ranking in terms of compressive strength and modulus was as follows: MLF/PVC foam > LF/PVC foam > PEG–IPDI/PVC foam > pure PVC foam. The compressive strength and modulus of the MLF/PVC foam were enhanced by 93.7% and 165.8%, respectively, compared to those of pure PVC foam (Figure 6b). The data indicates that MLF, with its multidirectional and hierarchical structure, enhances the mechanical properties of PVC foams. This enhancement is primarily attributed to MLF's ability to reinforce cell walls and struts. Additionally, the smaller cell size in the MLF/PVC foam contributes to a reduced bending moment in the cell walls during compressive deformation.[40]

Thermal energy storage capacity of MLF/PVC foam

The modification of LF with PEG–IPDI prepolymer transformed MLF into an SSPCM capable of thermal energy storage. Integrating MLF into PVC foam is theoretically beneficial for energy conservation and enhancing the foam's thermal insulation properties.[20-21] The thermal energy storage capacity of MLF/PVC foam was investigated by DSC analysis of the fillers and foams (Figures 7a–b), with corresponding thermal performance parameters summarized in Table II.

The DSC curves of LF showed no obvious endothermic or exothermic peaks, suggesting no phase change below 80°C (Figure 7a). However, PEG–IPDI prepolymer and MLF exhibited noticeable endothermic and exothermic peaks within the 0°–80°C range, indicating reversible thermal storage and release capabilities (Figure 7a). The phase change enthalpies (ΔH_m and ΔH_c) of MLF during melting and crystallization were lower than

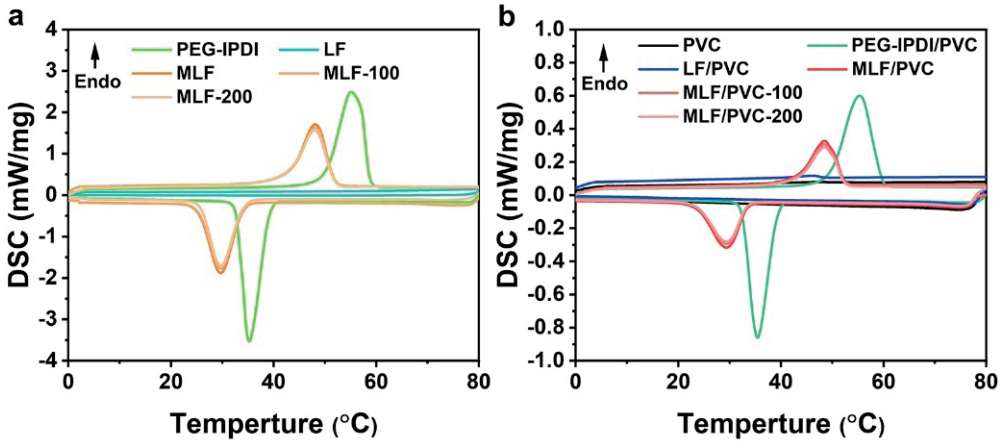

Figure 7. DSC curves of **(a)** fillers and **(b)** foams.

Table II

Thermal performance parameters of fillers and foams

	ΔH_m (J/g) [a]	T_m (°C) [a]	ΔH_c (J/g) [a]	T_c (°C) [a]
PEG-IPDI	170.1	55.2	164.2	35.2
LF	–	–	–	–
MLF	106.6	48.1	100.9	29.7
MLF-100 [b]	104.7	48.2	100.4	29.7
MLF-200 [b]	103.8	48.0	99.4	29.5
PVC	–	–	–	–
PEG-IPDI/PVC	48.6	55.0	44.3	35.3
LF/PVC	–	–	–	–
MLF/PVC	20.9	48.6	18.8	29.4
MLF/PVC-100 [b]	20.3	48.4	18.1	28.7
MLF/PVC-200 [b]	19.9	47.6	17.7	28.3

[a] ΔH_m and ΔH_c represent the phase change enthalpies during the melting and crystallization processes, respectively; T_m and T_c denote the melting and crystallization temperatures, respectively.

[b] MLF-100 and MLF-200 indicate MLF after 100 and 200 thermal cycles, respectively; MLF/PVC-100 and MLF/PVC-200 refer to MLF/PVC foam after 100 and 200 thermal cycles, respectively.

those of PEG–IPDI prepolymer (Figure 7a and Table II), suggesting a deterioration in thermal storage and release capabilities of MLF compared to those of PEG–IPDI prepolymer.[41-42] This is likely due to the cross-linked networks between LF and PEG–IPDI prepolymer restricts PEG chain movement. Despite this, the ΔH_m and ΔH_c values of MLF/PVC foam were maintained at 20.9 and 18.8 J/g, respectively, after incorporating MLF into PVC (Figure 7b), which contributes to energy savings and enhanced thermal insulation properties of the foam. Furthermore, the phase change enthalpies and temperatures for MLF and MLF/PVC foam remained relatively unchanged after 100 and 200 thermal cycles, demonstrating their excellent thermal reliability (Figure 7a and 7b and Table II).

Thermal insulation properties of MLF/PVC foam

As previously discussed, the MLF/PVC foam exhibits notable foaming and thermal energy storage capacities, which are expected to enhance its thermal insulation properties. Thermal conductivity is a critical metric for evaluating the thermal insulation properties of foams. Typically, the thermal conductivity of foams can be greatly reduced by increasing their expansion ratio.[43-44] Among the tested samples, MLF/PVC foam had the highest expansion rate, attributable to the improved foaming capacity imparted by MLF (Figure 5b). Consequently, MLF/PVC foam exhibited the lowest increase in thermal conductivity with rising temperature (25°–90°C) (Figure 8a). The thermal insulation properties were directly observed by placing samples on a heating plate at 110°C (Figure 8c), with infrared thermal images captured at different intervals (Figure 8d). MLF/PVC foam exhibited the slowest increase in surface temperature, suggesting that MLF effectively enhanced the thermal insulation properties of PVC foams by increasing their expansion rate.

Notably, the thermal conductivity of MLF (25°C, 1.7233 W/m·K) was higher than that of LF (25°C, 1.1905 W/m·K) (Figure 8b). While this might seem counterintuitive for enhancing thermal insulation, the similar thermal conductivity of MLF and PVC (25°C, 1.6951 W/m·K) allowed MLF/PVC foam to effectively utilize the thermal energy storage capacity of PEG during heat transfer. This was evidenced by the variations in thermal conductivity and surface temperature of MLF/PVC foam during the phase change interval (40°–50°C) in Figures 8a and 8c. Moreover, SEM observations of the sample cross-sections following impact fracture (Figure 8e) revealed that the multidirectional and hierarchical structure of MLF created numerous micropores and micro/nanofibrils in the cell walls. These micro/nanostructures enhance heat transfer path tortuosity and increase phonon scattering at micro/nanostructure boundaries, thereby reducing solid-phase thermal conduction.[45] In

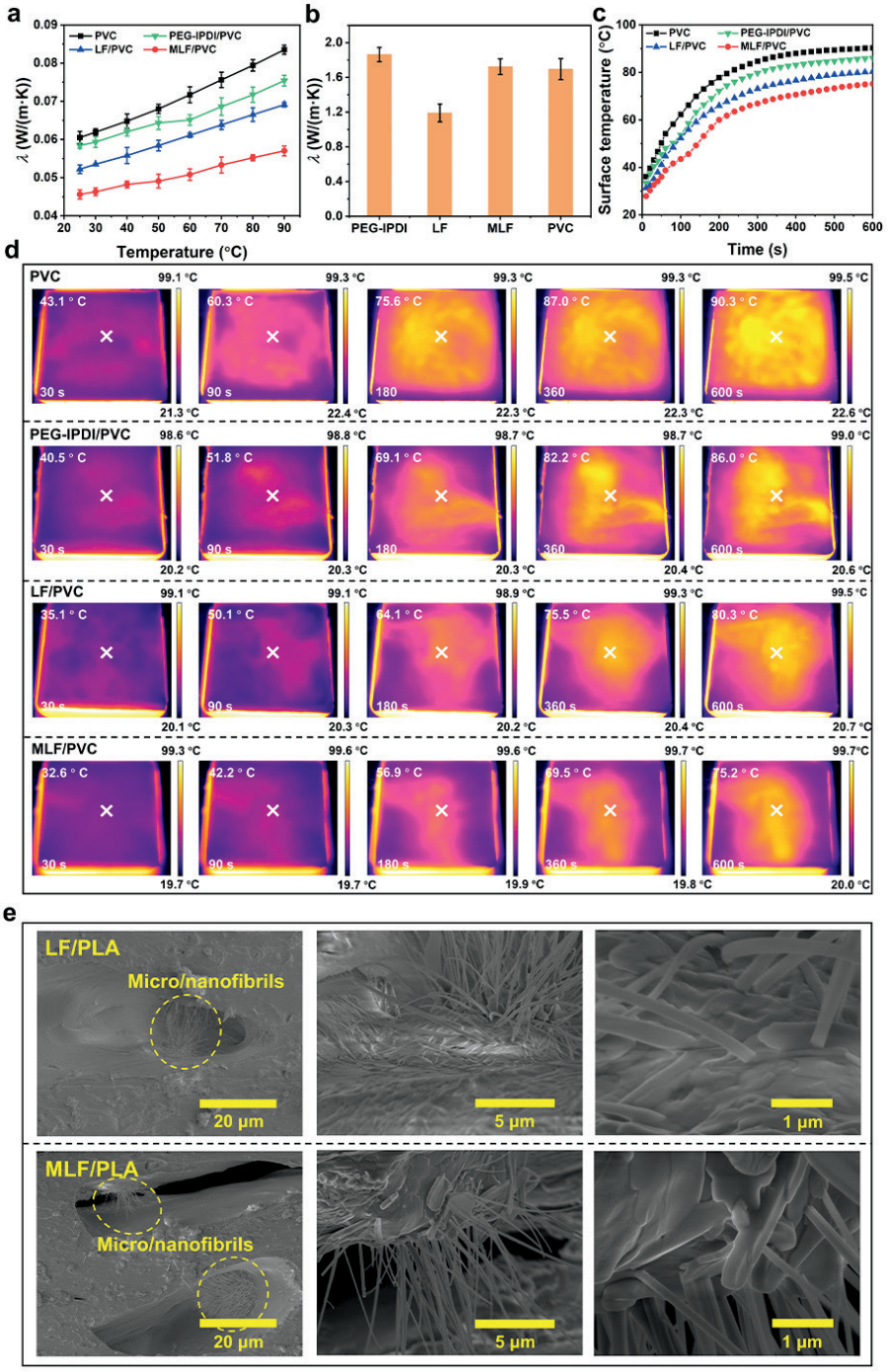

Figure 8. **(a)** Temperature-dependent thermal conductivity of pure PVC and composite foams; **(b)** thermal conductivity of fillers and PVC at 25°C; **(c)** surface temperature variations at the center point and **(d)** infrared thermal images of pure PVC and composite foams during 600 s of heating; **(e)** SEM images of the surfaces of LF/PVC and MLF/PVC foams.

summary, MLF enhances the thermal insulation properties of PVC foams through its improved foaming and thermal energy storage capacities.

Conclusion

This study demonstrated that the use of PEG–IPDI prepolymer effectively aligned the surface free energy of MLF with that of PVC, thereby enhancing their interfacial compatibility. This modification also endowed MLF with thermal energy storage capacity. Furthermore, MLF was shown to enhance the foaming capacity of PVC by increasing the melt's strength and viscoelasticity. Consequently, MLF/PVC foam exhibited a high expansion rate, small average pore diameter, and low density. These attributes collectively contributed to the notable improvement in both the mechanical and thermal insulation properties of PVC foams. The integration of MLF as a natural filler thus not only enhances the

properties of PVC foams but also presents a viable approach for the resourceful utilization of LSs. This work offers a promising direction for developing LF/PVC foam with superior mechanical and thermal insulation properties, utilizing the potential of LSs as a valuable resource.

Acknowledgement

This work was supported by the Fujian Provincial key science and technology project [2023YZ038001]. The authors acknowledge Dr. Ying Song, Dr. Xiu He, and Dr. Mi Zhou from the College of Biomass Science and Engineering of Sichuan University for their help in measurement and characterization.

References

1. Muralidharan, V., Palanivel, S., Balaraman, M.; Turning problem into possibility: A comprehensive review on leather solid waste intra-valorization attempts for leather processing. *J. Clean. Prod.* **367**, 133021, 2022.
2. Li, Y. C., Guo, R. J., Lu, W. H., Zhu, D. Y.; Research progress on resource utilization of leather solid waste. *J. Leather Sci. Eng.* **1**, 1-17, 2019.
3. Liu, J., Liu, Y. C., Brown, E. M., Ma, Z. X., Liu, C. K.; Fabrication of composite films based on chitosan and vegetable-tanned collagen fibers crosslinked with genipin. *JALCA* **116**, 345-358, 2021.
4. Peng, L. Q., Guo, L. J., Li, J. H., Zhang, W. H., Shi, B., Liao, X. P.; Rapid and highly selective removal of cesium by Prussian blue analog anchored on porous collagen fibers. *Sep. Purif. Technol.* **307**, 122858, 2023.
5. Ke, L., Zhao, K., Yan, X. Y., Cao, X. J., Wu, X. Y., Zhang, C., Luo, T. T., Ding, T., Yan, N.; Facile mineralization and valorization of Cr-containing leather shavings for electrocatalytic H_2O_2 generation and organic pollutant removal. *Chem. Eng. J.* **437**, 135036, 2022.
6. Li, S. Y., Shuai, P. Y., Wang, A. Q., Zhou, J. F., Shi, B.; Tailoring the interfacial interaction of collagen fiber/waterborne polyurethane composite via plant polyphenol for mechanically robust and breathable wearable substrate. *Compos. Part A-App. S.* **175**, 107810, 2023.
7. Xu, W. X., Wu, X. T., Shi, B.; Toughening agent for melamine formaldehyde resin: A new method for recycling chrome shavings. *Polymer* **253**, 124979, 2022.
8. Lei, C., Xu, W. X., Zeng, Y. H., Shi, B.; Study on interfacial compatibility and resilient creep resistance of silane-modified collagen fiber/polyvinyl chloride composites. *Acta Materiae Compositae Sinica* **42**, 1-12, 2023.
9. Guo, J., Dai, R., Chen, H., Liang, Y., Shan, Z. h.; Research on the composite and functional characteristics of leather fiber mixed with nitrile rubber. *J. Leather Sci. Eng.* **3**, 1-12, 2021.
10. Maou, S., Meghezzi, A., Grohens, Y., Meftah, Y., Kervoelen, A., Magueresse, A.; Effect of various chemical modifications of date palm fibers (DPFs) on the thermo-physical properties of polyvinyl chloride (PVC)–high-density polyethylene (HDPE) composites. *Ind. Crops Prod.* **171**, 113974, 2021.
11. Tang, Y., Zhang, W., Jiang, X. W., Zhao, J. Z., Xie, W. B., Chen, T.; Experimental investigations on phenomenological constitutive model of closed-cell PVC foam considering the effects of density, strain rate and anisotropy. *Compos. B Eng.* **238**, 109885, 2022.
12. Yao, K., Tan, H. Y., Lin, Y. C., Zhang, G. C., Gong, J., Qiu, J., Tang, T., Na, H., Jiang, Z. W.; Effect of polystyrene long branch chains on melt behavior and foaming performance of poly (vinyl chloride)/graphene nanocomposites. *RSC Adv.* **4**, 64053-64060, 2014.
13. You, J. A., Jiang, Z. W., Jiang, H. Q., Qiu, J., Li, M. G., Xing, H. P., Xue, J., Tang, T.; A "plasticizing-foaming-reinforcing" approach for creating thermally insulating PVC/polyurea blend foams with shape memory function. *Chem. Eng. J.* **450**, 138071, 2022.
14. Dewan, M., Adhikari, A., Chattopadhyay, D., Polyvinyl chloride foam. In Polymeric Foams: Fundamentals and Types of Foams (Volume 1), American Chemical Society, Washington, Vol. 1439, pp 237-256, 2023.
15. Khoshnoud, P., Abu-Zahra, N.; Properties of rigid polyvinyl chloride foam composites reinforced with different shape fillers. *J. Thermoplast. Compos. Mater.* **30**, 1541-1559, 2017.
16. Xu, L. F., Han, T., Li, J., Xiong, Y., Guo, S. Y.; The cell growth-induced orientation of mica in lightweight flexible poly (vinyl chloride) foams and its enhancement on sound insulation. *Compos. Sci. Technol.* **145**, 78-88, 2017.
17. Allahbakhsh, A.; PVC/rice straw/SDBS-modified graphene oxide sustainable nanocomposites: Melt mixing process and electrical insulation characteristics. *Compos. Part A-App. S.* **134**, 105902, 2020.
18. Zhang, T. R., Zeng, S. L., Jiang, H., Li, Z. S., Bai, D. Y., Li, Y. J., Li, J. J., Interfaces; Leather solid waste/poly (vinyl alcohol)/polyaniline aerogel with mechanical robustness, flame retardancy, and enhanced electromagnetic interference shielding. *ACS Appl. Mater. Interfaces* **13**, 11332-11343, 2021.
19. Villasmil, W., Fischer, L. J., Worlitschek, J.; A review and evaluation of thermal insulation materials and methods for thermal energy storage systems. *Renew. Sustain. Energy Rev.* **103**, 71-84, 2019.
20. Gao, N., Tang, T., Xiang, H. X., Zhang, W. L., Li, Y. B., Yang, C. L., Xia, T., Liu, X. L.; Preparation and structure-properties of crosslinking organic montmorillonite/polyurethane as solid-solid phase change materials for thermal energy storage. *Sol. Energy Mater. Sol. Cells* **244**, 111831, 2022.
21. Amaral, C., Pinto, S., Silva, T., Mohseni, F., Amaral, J., Amaral, V., Marques, P., Barros-Timmons, A., Vicente, R.; Development of polyurethane foam incorporating phase change material for thermal energy storage. *J. Energy Storage* **28**, 101177, 2020.
22. Zhao, Y. L., Liu, T. R., Wei, Z. K., Yuan, A. Q., Chen, Y., Jiang, L., Lei, J. X., Fu, X. W.; Polymeric phase change material networks based on multi-telechelic polyethylene glycol-derived multimer structures for thermal energy storage. *Chem. Eng. J.* **462**, 142164, 2023.
23. Xia, Y. P., Li, Q. T., Ji, R., Zhang, H. Z., Xu, F., Huang, P. R., Zou, Y. J., Chu, H. L., Lin, X. C., Sun, L. X.; Multielement synergetic effect of boron nitride and multiwalled carbon nanotubes for the fabrication of novel shape-stabilized phase-change composites with enhanced thermal conductivity. *ACS Appl. Mater. Interfaces* **12**, 41398-41409, 2020.

24. Tian, C., Ning, J. Y., Yang, Y. Y., Zeng, F. H., Huang, L., Liu, Q., Lv, J. H., Zhao, F. Q., Kong, W. B., Cai, X. F.; Super tough and stable solid–solid phase change material based on π-π stacking. *Chem. Eng. J.* **429**, 132447, 2022.
25. Li, S. Y., Wang, Y. P., Xu, S. F., Xiang, Z. W., Xu, W. X., Shi, B.; Ultradurable superhydrophobic natural rubber-based elastomer enabled by modified multiscale leather collagen fibers. *Adv. Mater. Interfaces* **7**, 2000344, 2020.
26. Lei, C., Xu, W. X., Shi, B., Zeng, Y. H.; Construction of cross-linked networks in polylactic acid biocomposites by using vegetable oil-modified collagen fibers for improving anti-stress relaxation and toughness. *Ind. Crops Prod.* **210**, 118160, 2024.
27. Wu, G., Weng, Z., Li, J. Q., Zheng, Z. C., Wen, Z. X., Fang, W. Q., Zhang, Y., Zhang, N., Chen, G., Liu, X. H.; Body armor-inspired double-wrapped binder with high energy dispersion for a stable SiO_x anode. *ACS Appl. Mater. Interfaces* **15**, 34852-34861, 2023.
28. Li, S. Y., Wang, Y. P., Xu, W. X., Shi, B.; Natural rubber-based elastomer reinforced by chemically modified multiscale leather collagen fibers with excellent toughness. *ACS Sustainable Chem. Eng.* **8**, 5091-5099, 2020.
29. Wang, C., Dong, W. J., Li, A., Atinafu, D. G., Wang, G., Lu, Y. F.; The reinforced photothermal effect of conjugated dye/graphene oxide-based phase change materials: Fluorescence resonance energy transfer and applications in solar-thermal energy storage. *Chem. Eng. J.* **428**, 130605, 2022.
30. Liu, W., Zhu, Y. F., Qian, C., Dai, H. B., Fu, Y. Q., Dong, Y. B.; Interfacial modification between glass fiber and polypropylene using a novel waterborne amphiphilic sizing agent. *Compos. B Eng.* **241**, 110029, 2022.
31. Hezma, A. M., Elashmawi, I. S., Abdelrazek, E. M., Rajeh, A., Kamal, M.; Enhancement of the thermal and mechanical properties of polyurethane/polyvinyl chloride blend by loading single walled carbon nanotubes. *Prog. Nat. Sci.: Mater. Int.* **27**, 338-343, 2017.
32. Hezma, A. M., Elashmawi, I. S., Rajeh, A., Kamal, M.; Change Spectroscopic, thermal and mechanical studies of PU/PVC blends. *Phys. B: Condens. Matter* **495**, 4-10, 2016.
33. Ali, I., Yang, W. M., Li, X. D., Ali, A., Jiao, Z. W., Xie, P. C., Dias, O. A. T., Pervaiz, M., Li, H. Y., Sain, M.; Highly electro-responsive plasticized PVC/FMWCNTs soft composites: A novel flex actuator with functional characteristics. *Eur. Polym. J.* **126**, 109556, 2020.
34. Ren, Q., Wu, M. H., Wang, L., Zheng, W. G., Hikima, Y., Semba, T., Ohshima, M.; Cellulose nanofiber reinforced poly (lactic acid) with enhanced rheology, crystallization and foaming ability. *Carbohydr. Polym.* **286**, 119320, 2022.
35. Lyu, Y., Pang, J. G., Gao, Z. J., Zhang, Q. L., Shi, X. Y.; Characterization of the compatibility of PVC/PLA blends by aid of rheological responses. *Polymer* **176**, 20-29, 2019.
36. Li, Y., Yin, D. X., Liu, W., Zhou, H. F., Zhang, Y. X., Wang, X. D.; Fabrication of biodegradable poly (lactic acid)/carbon nanotube nanocomposite foams: Significant improvement on rheological property and foamability. *Int. J. Biol. Macromol.* **163**, 1175-1186, 2020.
37. Mehrabi Mazidi, M., Edalat, A., Berahman, R., Hosseini, F. S.; Highly-toughened polylactide- (PLA-) based ternary blends with significantly enhanced glass transition and melt strength: Tailoring the interfacial interactions, phase morphology, and performance. *Macromolecules* **51**, 4298-4314, 2018.
38. Qiao, Y. H., Li, Q., Jalali, A., Yang, J. N., Wang, X. F., Zhao, N., Jiang, Y. C., Wang, S. W., Hou, J. H., Jiang, J.; In-situ microfibrillated poly (ε-caprolactone)/poly (lactic acid) composites with enhanced rheological properties, crystallization kinetics and foaming ability. *Compos. B Eng.* **208**, 108594, 2021.
39. Zhao, J. C., Wang, G. L., Wang, C. D., Park, C. B.; Ultra-lightweight, super thermal-insulation and strong PP/CNT microcellular foams. *Compos. Sci. Technol.* **191**, 108084, 2020.
40. Wang, J. C., Chai, J. L., Wang, G. L., Zhao, J. C., Zhang, D. M., Li, B., Zhao, H. B., Zhao, G. Q.; Strong and thermally insulating polylactic acid/glass fiber composite foam fabricated by supercritical carbon dioxide foaming. *Int. J. Biol. Macromol.* **138**, 144-155, 2019.
41. Alva, G., Lin, Y. X., Fang, G. Y.; Synthesis and characterization of chain-extended and branched polyurethane copolymers as form stable phase change materials for solar thermal conversion storage. *Sol. Energy Mater. Sol. Cells* **186**, 14-28, 2018.
42. Du, X. S., Qiu, J. H., Deng, S., Du, Z. L., Cheng, X., Wang, H. B.; Flame-retardant and solid-solid phase change composites based on dopamine-decorated BP nanosheets/Polyurethane for efficient solar-to-thermal energy storage. *Renewable Energy* **164**, 1-10, 2021.
43. Song, L. M., Chen, Y. Q., Gao, Q. C., Li, Z., Zhang, X. Y., Wang, H. L., Guan, L., Yu, Z. J., Zhang, R., Fan, B. B.; Low weight, low thermal conductivity, and highly efficient electromagnetic wave absorption of three-dimensional graphene/SiC-nanosheets aerogel. *Compos. Part A-App. S.* **158**, 106980, 2022.
44. Jia, L. J., Phule, A. D., Yu, Z., Zhang, X., Zhang, Z. X.; Ultra-light poly(lactic acid)/SiO_2 aerogel composite foam: A fully biodegradable and full life-cycle sustainable insulation material. *Int. J. Biol. Macromol.* **192**, 1029-1039, 2021.
45. Noroozi, M., Panahi-Sarmad, M., Abrisham, M., Amirkiai, A., Asghari, N., Golbaten-Mofrad, H., Karimpour-Motlagh, N., Goodarzi, V., Bahramian, A. R., Zahiri, B.; Nanostructure of aerogels and their applications in thermal energy insulation. *ACS Appl. Energy Mater.* **2**, 5319-5349, 2019.